Star-forming galaxies at $z \sim 0.61$

Carlos Gómez-Guijarro[1], Jesús Gallego[1], Lucía Rodríguez-Muñoz[1], Víctor Villar[1], Jean-Gabriel Cuby[2], and Benjamin Clément[3]

[1] Dpto. de Astrofísica y CC. de la Atmósfera. Facultad de CC. Físicas, Universidad Complutense de Madrid, Av. Complutense s/n. E-28040, Madrid, Spain
[2] Aix Marseille Université, CNRS, LAM (Laboratoire d'Astrophysique de Marseille) UMR 7326, 13388, Marseille, France
[3] CRAL, Observatoire de Lyon, CNRS, Université Lyon 1, 9 Avenue Ch. Andr, F-69561 Saint Genis Laval Cedex, France

Abstract

In this work we have studied a sample of 41 galaxies with active star formation at $z \sim 0.61$ selected by their emission in Hα+[N II]$\lambda\lambda$6548,6584 in ultradeep images (32 h of exposure time) taken with a narrow-band filter in the near-infrared with HAWK-I instrument on the VLT. The aim is to characterize the physical and global properties of this sample of galaxies. We have calculated the luminosity function. Our determination of $\alpha = -1.29 \pm 0.02$ is the deepest to date in similar studies. This leads to a star formation rate density $\mathrm{SFRd} = 0.10 \pm 0.01 \, \mathrm{M_\odot \, yr^{-1} \, Mpc^{-3}}$. We have found a correlation between extinction and star formation rate (SFR) and between SFR and stellar mass in the sample. We have performed a morphological and spectroscopical classification of the objects studying the physical properties of the categories. Disks have the highest SFR, but BCDs form stars at the same rate in terms of specific star formation rate (sSFR). Excitation decreases and luminosity increases with the spectroscopic class.

1 Introduction

The study of the galaxy population of the Universe requires a series of observables to compare the different physical properties along its history. One of these observables is the star formation rate density (SFRd). The SFRd has been a topic of study in the last decades. Since the first work [21] to the present day different results have been obtained up to $z \sim 10$ employing several tracers from X-rays to radio emission [14]. The cosmic SFRd grows from the origin of the first galaxies and peaks at $z \sim 2 - 3$ [20]. It becomes constant up to $z = 1$ and then falls down 10-20 times to $z = 0$ [11].

The objetive of this work is to determine the SFRd at $z \sim 0.61$ and to study global and physical properties of star-forming galaxies (SFGs) at $z \sim 0.61$. In order to do this, we employ Hα as a tracer of the instantaneous star formation rate [15]. We make use of a narrow-band (NB) filter to select the SFGs by their emission lines.

This project complements previous studies carried out by the UCM group using Hα at different redshifts [11, 24, 25, 34].

Throughout this work we adopt a cosmology with $[\Omega_\Lambda, \Omega_M, h] = [0.7, 0.3, 0.7]$. Considering these parameters the age of the Universe at z=0.61 is 7.69 Gyr, the luminosity distance is 3601.6 Mpc and the scale 6.736 kpc/arcsec. AB magnitude system is employed over the whole study.

2   Sample selection

The data used in this work correspond to very deep observations in the GOODS-S field with VLT HAWK-I imager [17, 30]. A NB filter centered at $1.061\,\mu$m (*NB1060*) was employed. The data was obtained as part of an ESO large programme that was aimed to detect Lyman-alpha emitters (LAEs) at $z = 7.7$ in order to constrain the epoch of reionization (project 181.A-0485(A), [7]). These deep images provide secondary observations of Hα emitters at $z \sim 0.61$ that we employ in this work.

Emission-line objects were selected by comparing apparent fluxes in the NB with a broad-band (BB). Those candidates with intense emission line present a flux excess in the NB filter, compared to the BB flux. The selection process was performed using the technique described in [26]. We got a total sample of 46 candidates to emission-line emitters.

In addition, we employed photometric and spectroscopic ancillary data. From CAN-DELS [13, 18] we collected astrometry, photometric redshifts, spectroscopic redshifts, masses, sizes and various synthetic data. From the literature we found 7 optical spectra [19, 32, 4]. We checked the original sample for the total of 46 candidates to emission-line emitters. 42 of them had counterpart in the CANDELS database, being confirmed as galaxies. We looked for the four with no counterpart in the CANDELS multicolor Interactive Display[1]. Two of them leave the display field, another one was a star contaminated by a neighborhood object and the last one had no counterpart in the CANDELS images, either is an artefact or a very low luminosity line emitter. Spectroscopically, one of the 42 objects is confirmed as a Hβ emitter. Then, our final sample is composed of 41 objects.

We have developed a webpage of the sample[2]. The reader should find there all the data concerning each object of the sample, as well as RGB images and spectra, if it is available.

---

[1] http://archive.stsci.edu/prepds/candels/display_gs-tot_v1.0.html
[2] http://guaix.fis.ucm.es/node/1586

3 Fluxes, luminosities and extinction

In order to get Hα line and continuum fluxes we follow the [26] approach. After that, we compute the Hα line luminosity from $L = 4\pi d_{\mathrm{l}}^2(z)f_{\mathrm{l}}$. To determine the luminosity distance we employ the spec-z values if available, otherwise we take the average redshift $z = 0.61$.

Fluxes and luminosities are then corrected from extinction. We calculate the far ultraviolet (FUV) extinction as indicated in [5] from the ratio between dust and FUV fluxes ($F_{\mathrm{dust}}/F_{\mathrm{FUV}}$). We get F_{dust} from the total infrared (IR) luminosity synthetically calculated if IR data is available and F_{FUV} from synthetic FUV magnitude. For those objects with no IR data available we employ FUV and near ultraviolet (NUV) synthetic magnitudes, getting the ratio $F_{\mathrm{dust}}/F_{\mathrm{FUV}}$ as indicated in [22]. Finally, we obtain Hα extinction (A$_{\mathrm{H}\alpha}$) from a Calzetti extinction law [6].

4 Sample properties

We calculate the observed and extinction corrected Hα luminosity function (LF) with a V/V_{max} method [29]. Our interval redshift is $0.6098 < z < 0.6263$ with a comoving volume covered of $1222\,\mathrm{Mpc}^3$. We fit the result to a Schechter function [28, 11] $\phi(L)dL = \phi^*\left(\frac{L}{L^*}\right)^{\alpha}\exp\left(-\frac{L}{L^*}\right)\frac{dL}{L^*}$. The observed LF is then corrected using the extinction value for each object individually [34, 2]. The uncertainties in Schechter parameters are calculated performing Monte Carlo simulations.

In our study we can see a very well defined faint-end of the LF as a consequence of the extremely deep survey, with $32\,\mathrm{h}$ of integration time in the NB. Consequently, we have a flux detection limit $> 1.7 \times 10^{-18}\,\mathrm{erg\,s^{-1}\,cm^{-2}}$. On the other hand, the small field of the instrumentation for this kind of research leads us detect insufficient objects in the bright-end of the LF. We try to solve this issue extracting a sample in SDSS DR8 [1], with no results. We decide to simulate the number of galaxies in the bright bins. Firstly, we calculate a preliminar value of the α parameter via linear fitting of the faint-end. Secondly, we predict the SFRd at $z = 0.61$ from [34] expression SFRd $= A(1 + z)^{3.8}$. Assuming that the change in the SFRd evolution is not due to a change in the number of objects from $z = 0.84$ to $z = 0.61$, we can fix the value of ϕ^* and obtain L^*. With the three parameters of the Schechter function calculated for $z = 0.61$, we integrate the LF to get the bright-end bins. Once we have the complete version of the LF built with observed faint bins and simulated bright bins, we fit it to the Schechter function getting the values at $z \sim 0.61$: $\phi^* = 10^{-2.77\pm0.05}\,\mathrm{Mpc^{-3}}$; $L^* = 10^{42.78\pm0.02}\,\mathrm{erg\,s^{-1}}$; $\alpha = -1.29 \pm 0.02$. In Fig. 1 we show the LF of this work along with other studies at different redshifts. Through [16] we get a value of SFRd $= 0.10 \pm 0.01\,\mathrm{M_\odot\,yr^{-1}\,Mpc^{-3}}$.

5 Physical properties

It is very interesting to study the properties of galaxies and their mutual relations. One of the properties we can study is extinction and its relation with SFR as we show in Fig. 2 (left).
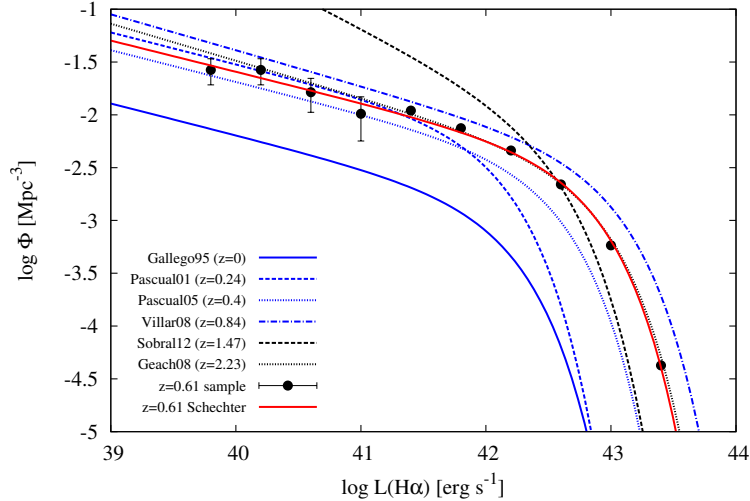
Figure 1:   Comparison with similar Hα studies: [11], [24], [25], [31], [12] as it is indicated in the legend.

The more the SFR the greater the obscuration. We see there is an apparent linear relation. However, the selection effects cause differences. The objects of this work that overlap with the characteristics of the $z = 0.84$ galaxies are disks. The remaining objects plotted at $z = 0.61$ trace a different galaxy population. Our survey cover a deep and small field, then, we do not see many disks due to a lack of area and we see a high number of small galaxies with low SFR.

Another property we can study is the stellar mass and its relation with SFR (see Fig. 2; middle). The galaxies with higher star formation are the ones with higher mass [23, 27, 35]. We see that our objects are below the expected trend [35]. We interpret this as a consequence of the galaxy population we are observing. They are UV-bright and very low-mass galaxies, much less massive than those in [35] which have a mass completeness limit $> 10^{9.6} \, \mathrm{M_\odot}$ in the redshift interval $0.5 < z < 1.0$, so we are seeing a different population. In terms of sSFR, it decreases with mass (see Fig. 2; right).

6   Morphological and spectroscopical classifications

Using RGB images from HST ACS, we classify our sample in morphological terms. In addition, we study the physical properties of the categories (see Table 1). We can see that, for this sample, spirals are the largest and most massive with a highest SFR. Disk galaxies are smaller than previous ones and have lower SFR. We can interpret them as a small version of the first ones. BCD are very compact and low-mass galaxies, however they have a high
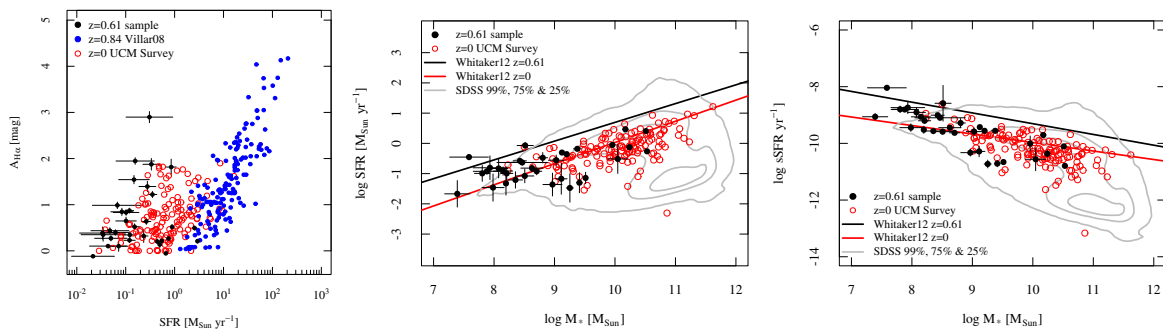
Figure 2: *Left* panel: Hα extinction versus SFR. This work is shown with black filled circles, the UCM Survey ($z = 0$) in red open circles and [34] ($z = 0.84$) in blue filled circles. *Center* panel: SFR versus stellar mass. This work in black filled circles and UCM survey in red open circles. SDSS galaxies are shown as a reference in grey contours. Main sequence of SFGs at $z = 0.61$ as a black line along with red line at $z = 0$ from [35]. *Right* panel: sSFR versus stellar mass following center panel code.

SFR for its size, much larger than irregulars and similar to disk galaxies that are much larger and more massive. Apart from this, we observe a growing relation in extinction with the morphological category from spirals to BCD. The last ones evidence a strong star formation environment, showing sSFR very high and close to those in spirals. BCD are compact, low-mass and starburst systems.

Table 1: Physical properties for our morphological categories. The columns show the values: (1) category; (2) rest-frame Hα equivalent width in Å; (3) Hα extinction in magnitudes; (4) extinction corrected star formation rate in $M_\odot \, yr^{-1}$; (5) extinction corrected specific star formation rate in Gyr^{-1}; (6) stellar mass in $\log M_\odot$; (7) diameter in kpc.

Category	EW_{rf}	$A_{H\alpha}$	SFR_{cor}	$sSFR_{cor}$	Mass	Diameter
Spirals	27±16	0.28±0.19	1.4±1.1	4.8±7.8	9.4±1.1	15.3±5.3
Disk galaxies	20±16	0.56±0.59	0.27±0.20	1.1±2.0	8.95±0.57	13.2±7.3
Irregulars	34±31	0.69±0.81	0.11±0.10	0.9±1.8	8.82±0.81	8.6±4.0
BCD	156±190	1.06±0.61	0.26±0.24	3.0±3.9	8.07±0.54	4.9±1.6
Uncertain	567±1100	1.08±0.43	0.095±0.051	0.8±1.5	8.68±0.78	5.5±2.9

In terms of spectroscopy, those galaxies with high [O III]/Hβ ratio, EW(Hα), EW(Hβ), EW([O II]) and low masses and sizes are classified as *HII-like*. Galaxies with low [O III]/Hβ ratio, EW(Hα), EW(Hβ), EW([O II]) and high masses and sizes are classified as *disk-like*. We add a third category for disk-like galaxies with low masses, *dwarf disk-like* galaxies. We plot some line-ratio diagnostic diagrams [3, 33]. We see that HII-like galaxies present higher excitation and lower luminosities. On the contrary, disk-like ones present lower excitation but higher luminosities (see Fig. 3; left). Dwarf disk-like types are located in a transition
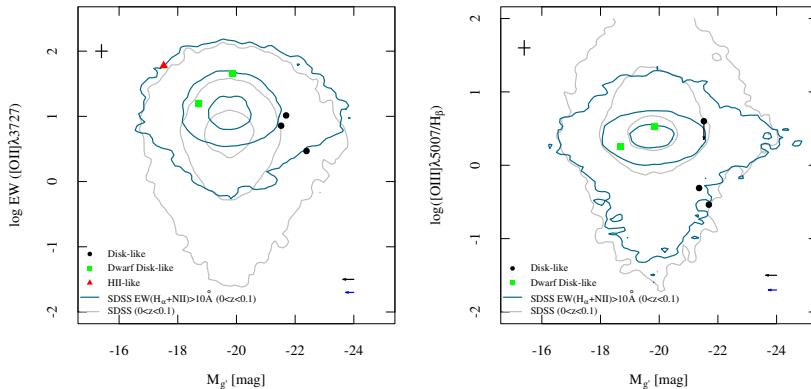
Figure 3: *Left* panel: excitation versus rest frame absolute *g'* magnitude. *Right* panel: EW([O II]) versus rest frame absolute *g'* magnitude. Spectroscopic classification is included as explained in the legend as well as the SDSS reference (grey contours 99%,75% and 25%). An estimation of the error is shown at the top left corner of each image. At the bottom right corner two arrows indicate the displacement considering rest frame *B* absolute magnitude instead of *g'* for the sample points (black arrow) and for the SDSS contours (blue arrow). The length is established through a typical galaxy color [8].

between this two types. These differences are also seen in Fig. 3 (right), as HII-like ones show higher EW([O II]) than disk-like.

7 Results and conclusions

In this work we have studied a sample of 41 galaxies with active star formation at $z \sim 0.61$ selected by their emission in Hα in ultradeep images taken with a NB filter in the near-infrared. We have calculated the LF corrected from extinction. Our determination of $\alpha = -1.29 \pm 0.02$ is the deepest to date in similar studies. This leads to a SFRd $= 0.10 \pm 0.01 \, M_\odot \, yr^{-1} \, Mpc^{-3}$. We have found a correlation between extinction and SFR, concluding that galaxies have higher extinction with increasing SFR [34, 2]. We have found a correlation between SFR and stellar mass, as the mass increases so does the SF [23, 27, 35]. The trend is the opposite in terms of sSFR. According to our morphological classification disks have the highest values of SFR, but BCDs form stars at the same rate in sSFR. Finally, spectroscopic study shows that excitation decreases and luminosity increases with the spectroscopic class [9, 10].

References

[1] Aihara, H., Allende Prieto, C., An, D., et al. 2011, ApJS, 193, 29

[2] An, F. X., Zheng, X. Z., Wang, W.-H., et al. 2014, ApJ, 784, 152

[3] Baldwin, J. A., Phillips, M. M., & Terlevich, R. 1981, PASP, 93, 5

[4] Balestra, I., Mainieri, V., Popesso, P., et al. 2010, A&A, 512, A12

[5] Buat, V., Iglesias-Páramo, J., Seibert, M., et al. 2005, ApJ, 619, L51

[6] Calzetti, D., Armus, L., Bohlin, R. C., et al. 2000, ApJ, 533, 682

[7] Clément, B., Cuby, J.-G., Courbin, F., et al. 2012, A&A, 538, A66

[8] Fukugita, M., Shimasaku, K., & Ichikawa, T. 1995, PASP, 107, 945

[9] Gallego, J., Zamorano, J., Rego, M., & Vitores, A. G. 1997, ApJ, 475, 502

[10] Guzmán, R., Gallego, J., Koo, D. C., et al. 1997, ApJ, 489, 559

[11] Gallego, J., Zamorano, J., Aragon-Salamanca, A., & Rego, M. 1995, ApJ, 455, L1

[12] Geach, J. E., Smail, I., Best, P. N., et al. 2008, MNRAS, 388, 1473

[13] Grogin, N. A., Kocevski, D. D., Faber, S. M., et al. 2011, ApJS, 197, 35

[14] Hopkins, A. M., & Beacom, J. F. 2006, ApJ, 651, 142

[15] Kennicutt, R. C., & Evans, N. J. 2012, ARA&A, 50, 531

[16] Kennicutt, Jr., R. C. 1998, ARA&A, 36, 189

[17] Kissler-Patig, M., Pirard, J.-F., Casali, M., et al. 2008, A&A, 491, 941

[18] Koekemoer, A. M., Faber, S. M., Ferguson, H. C., et al. 2011, ApJS, 197, 36

[19] Le Fèvre, O., Vettolani, G., Paltani, S., et al. 2004, A&A, 428, 1043

[20] Madau, P., & Dickinson, M. 2014, ArXiv e-prints, arXiv:1403.0007

[21] Madau, P., Ferguson, H. C., Dickinson, M. E., et al. 1996, MNRAS, 283, 1388

[22] Muñoz-Mateos, J. C., Gil de Paz, A., Boissier, S., et al. 2009, ApJ, 701, 1965

[23] Noeske, K. G., Weiner, B. J., Faber, S. M., et al. 2007, ApJ, 660, L43

[24] Pascual, S., Gallego, J., Aragón-Salamanca, A., & Zamorano, J. 2001, A&A, 379, 798

[25] Pascual, S. 2005, PASP, 117, 120

[26] Pascual, S., Gallego, J., & Zamorano, J. 2007, PASP, 119, 30

[27] Rodighiero, G., Daddi, E., Baronchelli, I., et al. 2011, ApJ, 739, L40

[28] Schechter, P. 1976, ApJ, 203, 297

[29] Schmidt, M. 1968, ApJ, 151, 393

[30] Siebenmorgen, R., Carraro, G., Valenti, E., et al. 2011, The Messenger, 144, 9

[31] Sobral, D., Best, P. N., Matsuda, Y., et al. 2012, MNRAS, 420, 1926

[32] Vanzella, E., Cristiani, S., Dickinson, M., et al. 2008, A&A, 478, 83

[33] Veilleux, S., & Osterbrock, D. E. 1987, ApJS, 63, 295

[34] Villar, V., Gallego, J., Préz-González, P. G., et al. 2008, ApJ, 677, 169

[35] Whitaker, K. E., van Dokkum, P. G., Brammer, G., & Franx, M. 2012, ApJ, 754, L29